Recent Results From Crystal Barrel

Michael Doser
CERN / PPE
1211 Genève 23, Switzerland
on behalf of the Crystal Barrel collaboration

Abstract. The Crystal Barrel experiment has continued its program to clarify the nature of low mass resonances. Results from high multiplicity final states, final states containing kaons (partly rendered possible by a hardware upgrade - a silicon microstrip detector), and annihilation in flight (in which the rest frame energy is extended up to 2.4 GeV) are presented. In addition, several tests of chiral perturbation theory, using $\bar{p}p$ annihilation as a meson factory, are summarized.

ANNIHILATION AT REST

The Crystal Barrel experiment has accumulated very large data samples in a large number of final states in the gluon-rich environment of $\bar{p}p$ annihilation. Partial wave analyses of individual final states, or coupled channel analyses of several final states [1] have led to the observation of several scalar states: the isoscalar states $f_0(1370)$ and $f_0(1500)$, as well as the isovector state $a_0(1450)$. The determination of the coupling of these mesons to kaonic final states is of fundamental importance to establish their nature.

In order to strongly enhance the capability of the Crystal Barrel detector to trigger on events containing secondary vertices (i.e. $K_S \to \pi^+\pi^-$), a silicon microstrip detector was built to closely surround the target region [2]. In addition to enhancing the statistics of events containing one or more kaons by a factor of 100 over minimum bias data, the detector also improves the momentum resolution of charged particles by 40 %. A total of 3.5 M events containing a K_S or a Λ with different targets was recorded, leading to statistics of about 50 k events per three-body final state containing a K_S.

A first analysis depending on this detector is a measurement of the Pontecorvo reactions $\bar{p}d \to K^0\Lambda$ and $\bar{p}d \to K^0\Sigma$. These reactions can be observed in the Crystal Barrel for both K_S and K_L, and for both charged and neutral decay modes of the K_S and the Λ, thus allowing a good control of the systematic errors on the measured branching rations. Starting from a total of

4.6×10^6 triggers (corresponding to about 5×10^8 annihilations in lD_2), events containing secondary vertices coming either from K_S or Λ decays are selected. The resulting invariant mass spectrum is shown in Fig. 2a). Requiring that no activity is observed in the calorimeter (i.e. from additional photons) leads to the K_S and Λ momentum distributions in Fig. 2b) and c), in which the Pontecorvo reactions are visible. If instead, one photon is detected in the calorimeter, Σ candidates are found, whose momentum distribution (Fig. 3a) indicates a signal at the expected momentum of 1090 MeV/c for the reaction $\bar{p}p \to K_L\Sigma$. Indeed, selecting events with a momentum larger than 950 MeV, and plotting the $\Lambda\gamma$ invariant mass shows a background-free Σ signal (Fig. 3b). Also in the case of two secondary vertices from the reaction $\bar{p}p \to K_S\Lambda\gamma$ with no additional activity in the calorimeter, a signal for the Pontecorvo reaction $\bar{p}p \to K_S\Sigma$ is seen in the K_S vs. Σ momentum distribution of Fig. 3c).

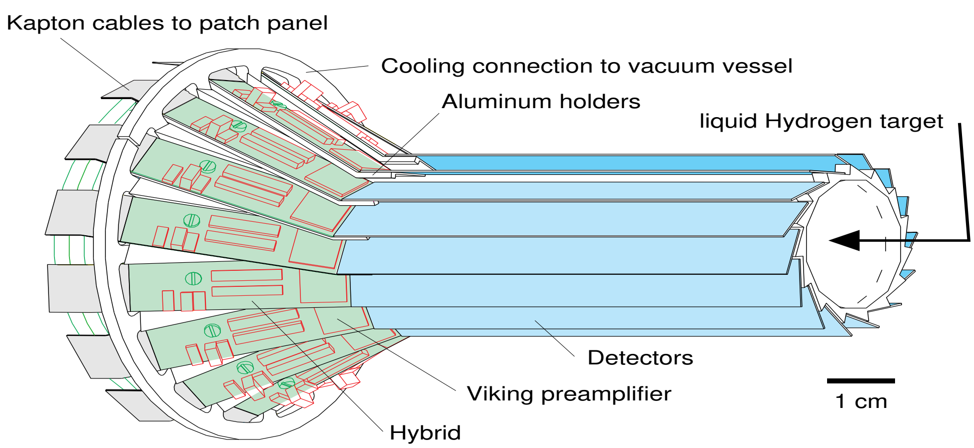

FIGURE 1. Schematic overview of the silicon microstrip detector.

Recently, the channel $\bar{p}p \to K_LK_L\pi^0$ has been observed (Fig. 4a) and a spin parity analysis performed by the Crystal Barrel experiment [3]. Contrary to previous bubble chamber experiments which only gave an upper limit [4] for the presence of a scalar state at 1500 MeV, this analysis with greatly increased statistics finds a non-zero signal for $f_0(1500) \to \bar{K}K$. The intensity of this state is closely coupled to that of a further state present in the same Dalitz plot, the $a_0(1450)$. In order to establish the relative intensities of the two states, input from another channel ($\bar{p}p \to K_LK^\pm\pi^\mp$) is necessary, in which only the $a_0(1450)$ can be seen. A complete presentation of the analysis of this channel can be found in the contribution of M. Heinzelmann to these proceedings. The quality of the Dalitz plot fit as a function of the contribution of the $a_0(1450)$ is shown in Fig. 4b), where a clear minimum in χ^2 indicates the most probable contribution, thus establishing the absolute rate of $f_0(1500) \to \bar{K}K$.

The same states could in principle be observed in another kaonic channel,

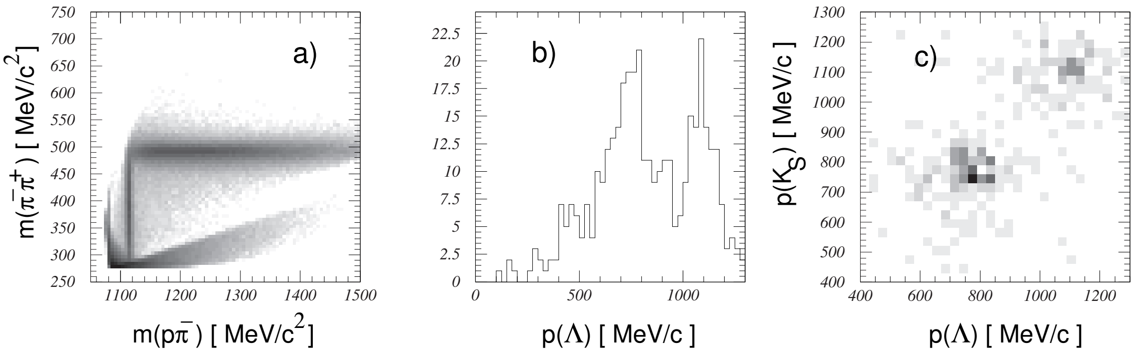

FIGURE 2. a) Invariant mass distribution for secondary vertices. Plotted is the value of one mass assignment ($\pi\pi$) against the value of the other mass assignment ($p\pi$). b) Λ momentum distribution for $K_L\Lambda$ events. c) K_S momentum vs Λ momentum for events containing two secondary vertices and no activity in the barrel.

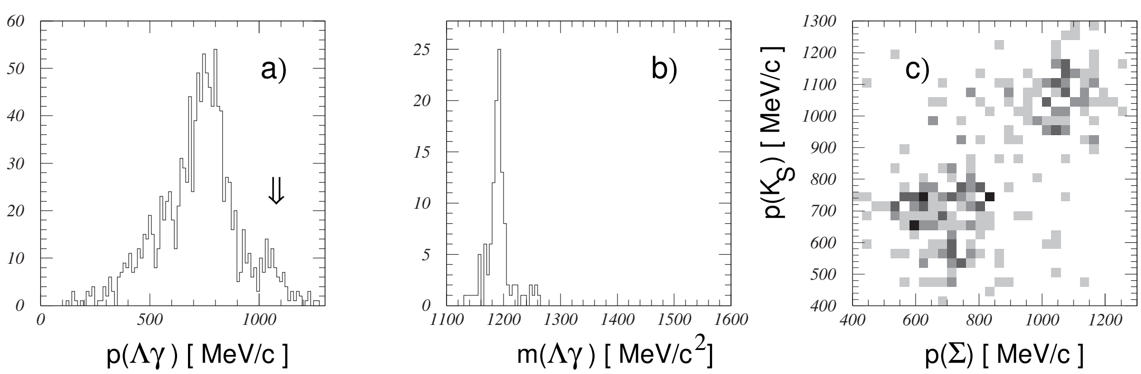

FIGURE 3. a) Momentum distribution of candidate Σ baryons in the reaction $\bar{p}p \to K_L\Lambda\gamma$ (no further activity in the barrel). The arrow indicates the expected Σ momentum for $\bar{p}d \to \Sigma K$ events. b) Invariant $\Lambda\gamma$ mass distribution for Σ candidates in a) if their momentum is greater than 950 MeV/c. c) K_S momentum vs Σ momentum for $K_S\Lambda\gamma$ events with no further activity in the calorimeter, and where both K_S and Λ decay into two charged particles.

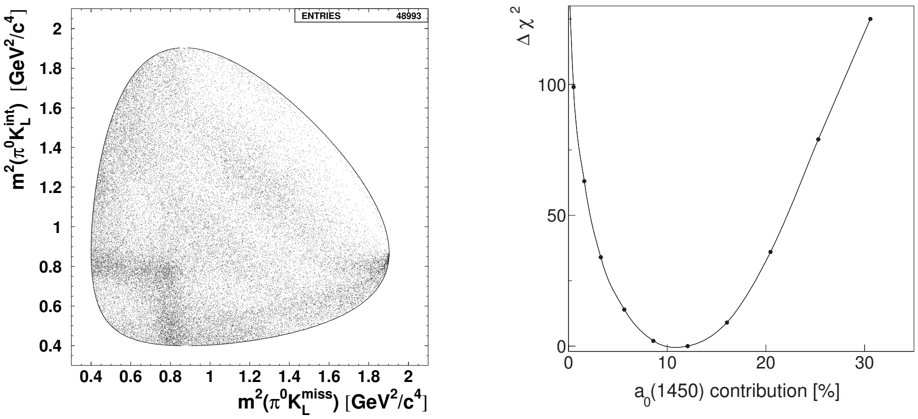

FIGURE 4. a) Dalitz plot for the reaction $\bar{p}p \to K_L K_L \pi^0$. b) Quality of fit to the $K_L K^\pm \pi^\mp$ Dalitz plot as a function of the $a_0(1450)$ contribution.

$\bar{p}p \to K^+K^-\pi^0$. The experimental Dalitz plots, consisting of 27200 events, is shown in Fig. 5a). The dashed lines indicate $m(\bar{K}K) = 1.3$ and 1.5 GeV/c^2. A partial wave analysis shows that in this reaction, the $\pi^0(KK)_S, KK^*(892)$ and $\pi^0\phi(1020)$ intermediate states dominate. Weak signals are observed for $\pi^0 a_2(1320)$, $\pi^0 f_2(1270), \pi^0 f_2'(1525)$ and $K(K\pi)_S$. The quality of this fit is shown in Fig. 5b). Discrepancies remain in the K^+K^- spectrum around 2, 2.4 and 2.7 GeV$^2/c^4$. A fully satisfactory description of the Dalitz plot is only possible through the introduction of a $(KK)_P$ wave with at least one high mass pole, corresponding to $\omega(1600)$, $\phi'(1680)$ or $\rho(1700)$. Although an attempt was made to fit the structure around 1700 MeV with a scalar or tensor, neither possibility was accepted by the fit, which clearly requires a vector meson in this mass range (the χ^2/dof improves from 1.5 to 1.18 when including two poles in the $(KK)_P$ wave). Also the $a_0(1450)$ was proposed to the fit (with fixed mass and width), which can accomodate a rate up to 20 % without changing the quality of the fit nor the contributions of the other amplitudes significantly. An upper limit for $a_0(1450)$ production and decay into K^+K^- is obtained: BR($\bar{p}p \to a_0(1450)$)$\times$ BR($a_0 \to K^+K^-$) $< (5.4 \pm 0.4) \times 10^{-4}$. With this channel, all kaonic three-body final states at rest have been separately analyzed by Crystal Barrel.

ANNIHILATION IN FLIGHT

As an extension of the previous channel to higher energies, Crystal Barrel has studied the reaction $\bar{p}p \to K^+K^-\pi^0$ at a c.m. energy of 2.4 GeV/c^2, by annihilating antiprotons of 1.9 GeV/c on the same liquid Hydrogen target as for annihilations at rest. Although a fraction of the events are kinematically

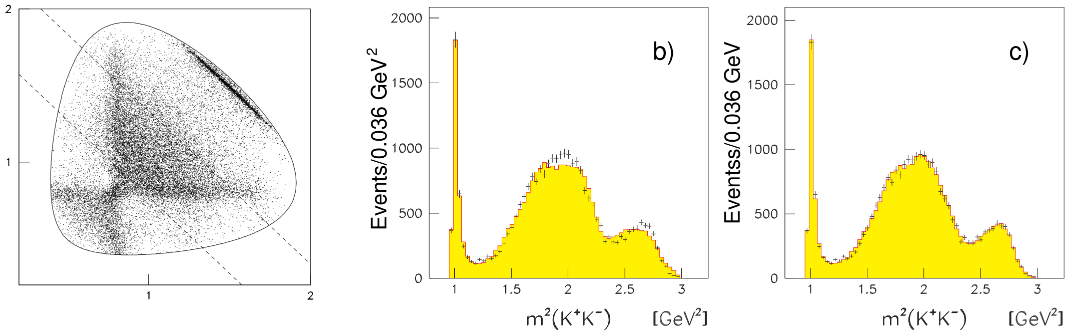

FIGURE 5. a) Dalitz plot for $K^+K^-\pi^0$ events for annihilation at rest. b) invariant (K^+K^-) mass distribution, data and fit without the $(K^+K^-)_P$ wave superimposed. c) invariant (K^+K^-) mass distribution, data and best fit (with the $(K^+K^-)_P$ wave) superimposed.

incomplete due to the forward boost and incomplete angular coverage of the detector, a total of 4290 kinematically complete $K^+K^-\pi^0$ events could be selected out of a total event sample of 47 $\times 10^6$ triggers (requiring the detection of two charged tracks). The Dalitz plot for these events (shown in Fig. 6a) shows a number of structures which are included in the fit. In the $(K\pi)$ mass distribution, the only visible structures are the K*(892) and the K$^*{}_{0/2}$(1430). In the (KK) mass distribution, there are enhancements around $\phi(1020)$ and $f_2(1270)$, as well as around 1500, 1700 and 1900 MeV. The quality of the fit with the above resonances is visible in the mass projections in Fig. 6 b) and c).

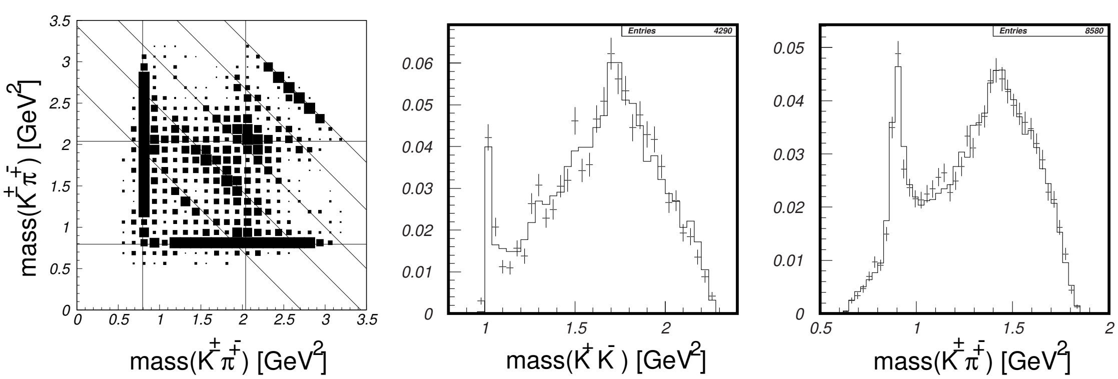

FIGURE 6. a) Dalitz plot for $K^+K^-\pi^0$ events for inflight annihilation ($p_{\bar{p}}$ = 1940 MeV/c). b) invariant (K^+K^-) mass distribution, data and best fit superimposed. c) invariant $(K^\pm\pi^\mp)$ mass distribution, data and best fit superimposed.

A second channel studied at 1940 MeV/c is the reaction $\bar{p}p \to \eta\eta\pi^0$. Here, 5832 events are selected from 7.7 $\times 10^6$ events which were recorded by triggering on activity in the barrel only. The structures visible in the Dalitz plot (Fig. 7a) are associated with the $a_0(980)$ and the $a_2(1320)$ in the $\eta\pi^0$ projections, and the $f_2(1270)$ and the $f_0(1500)$ in the $\eta\eta$ projection. Since an adequate description of the $a_0(980)$-crossing region, corresponding to high $\eta\eta$ invariant masses is difficult, the fit to the Dalitz plot is performed in two steps. In a first step, only the region with $m_{\eta\eta} < 3.8 GeV^2$ is fit. The above resonances give an acceptable fit. Several further resonances (i.e. $f_J(1700), \hat{\rho}_1(1440), a_2(1650)$) were proposed to the fit, but with the exception of the $a_2(1650)$, which improves the quality of the fit, they are rejected. The comparison between fit and data is shown in Fig. 7b) and c). When extending the fit to the full Dalitz plot, a further resonance with a mass of 2140 MeV and a width of 270 MeV is required in order to obtain an adequate description of the $a_0(980)$-crossing region, although it is not yet possible to distinguish between spin 0 and spin 2. The resulting invariant mass spectra are shown in Fig. 7.

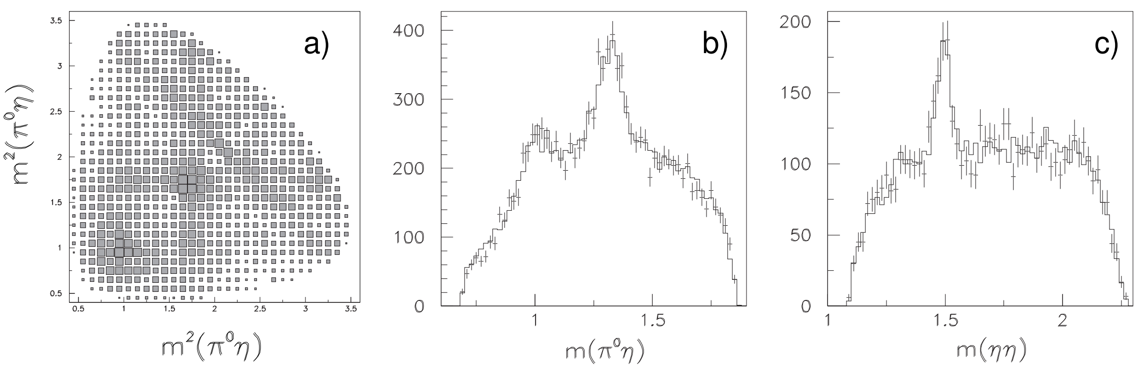

FIGURE 7. a) Dalitz plot for $\eta\eta\pi^0$ events for inflight annihilation ($p_{\bar{p}}$ = 1940 MeV/c). b) invariant ($\eta\eta$) mass distribution, data and best fit superimposed. c) invariant ($\eta\pi^0$) mass distribution, data and best fit superimposed.

These analyses show that the Crystal Barrel experiment has the data and the analysis techniques in hand to investigate the nature of such controversial states as the $f_J(1700)$ or the $\xi(2220)$. Work is in progress on analyzing the final states $3\pi^0$ (??? events) and $K^+K^-\pi^0$ (20'000 events) at 900 MeV/c (c.m. energy of 2049 MeV), as well as other Dalitz plots at a number of energies between 2049 MeV and 2400 MeV. Finally, data were taken in fine steps around 2230 MeV to search for a possible $\xi(2220)$ signal in the $\pi^0\pi^0$, $\eta\eta$ and possibly the $\eta\eta'$ cross sections.

TESTS OF QCD AND CHIRAL PERTURBATION THEORY

Antiproton-proton annihilation is a prolific source of mesons (π, η, η', ω) which are interesting in their own right. Chiral perturbation theory can be tested in η decays to $3\pi^0$ or $\pi^+\pi^-\pi^0$, SU(3) and $\rho-\omega$ mixing can be tested in rare radiative decays of ω, and the effects of the box anomaly can be detected by a study of the decay $\eta' \to \pi^+\pi^-\gamma$.

The first two analyses address η decays. Several chiral perturbation theory and current algebra predictions [5,6] for the calculation of the η decay into three pions, as well as experimental results [7,8] are in disagreement. The two reactions selected are $\bar{p}p \to \pi^0\pi^0\eta$ (with $\eta \to \pi^+\pi^-\pi^0$, 3230 events) and $\bar{p}p \to \pi^0\pi^0\eta$ (with $\eta \to 3\pi^0$). In the first case, the decay Dalitz plot of the η is analyzed in terms of the kinetic energy of the π^0. This distribution, described by a quadratic expression, is sensitive to a number of corrections beyond the d-quark–u-quark mass difference, in particular to final state interactions. Fig. 8 c) shows the intensity distribution as a function of the π^0 kinematic energy, with the superimposed fit. The fit determines the linear term to be a = -1.19 $\pm$ 0.07 and the quadratic term to be b = 0.19 $\pm$ 0.11 citemomdep. This is to be compared with the predictions from current algebra (a = -1.01, b = 0.26) [5], chiral perturbation theory (a = -1.30, b = 0.38) [5], and previous experiments : (a = -1.07$\pm$0.013, b=0) [8] and (a = -1.18$\pm$0.02, b = 0.20$\pm$0.03) [7].

The second η decay (into $3\pi^0$) is based on a larger (98'000 events) sample than the above reaction, and uses a different parametrization. Here, the amplitude of the transition matrix element M=A($\eta \to 3\pi^0$) is parametrized as $|M| \propto 1 + 2\alpha z$, where $z = \rho^2/\rho^2_{max}$ and ρ is the distance from the center of the decay Dalitz plot. Fig. 8 b) shows the amplitude squared $|M|^2$ as a function of z, again with a superimposed fit. The result of the fit (α = -0.052 $\pm 0.017_{stat} \pm 0.010_{sys}$ [10]) is the first indication of a negative α (previous experiments have obtained $\alpha = -0.022 \pm 0.023$ [13], resp. $\alpha = -0.32 \pm 0.37$ [14]), and is in agreement with predictions from chiral perturbation theory (α = -0.014, resp. -0.007, depending on the specific model used to calculate corrections beyond next-to-leading order in chiral perturbation theory [6]).

The rates of radiative meson decays can be predicted from SU(3) and the OZI rule [11], although these rates can be changed by SU(3) breaking by electromagnetism or quark masses [12]. In particular, the production and decay of the ρ and ω mesons is coupled by the isospin breaking ω to ρ transition. The effect of $\rho - \omega$ mixing is appreciable in processes with comparable ρ and ω production. Crystal Barrel measures the $\omega \to \eta\gamma$ branching ratio in two different reactions: $\bar{p}p \to \pi^0\omega$ and $\bar{p}p \to \eta\omega$. Since the relative production branching ratios ($\bar{p}p \to \eta\omega$)/ ($\bar{p}p \to \eta\rho$) and ($\bar{p}p \to \pi^0\omega$)/ ($\bar{p}p \to \pi^0\rho$) are very different [15], $\rho - \omega$ mixing is expected to lead to different values for $\omega \to \eta\gamma$ for the two ω production channels.

The 3-γ Dalitz plot for ω decays (Fig. 9) from the reaction $\bar{p}p \to \pi^0\omega$

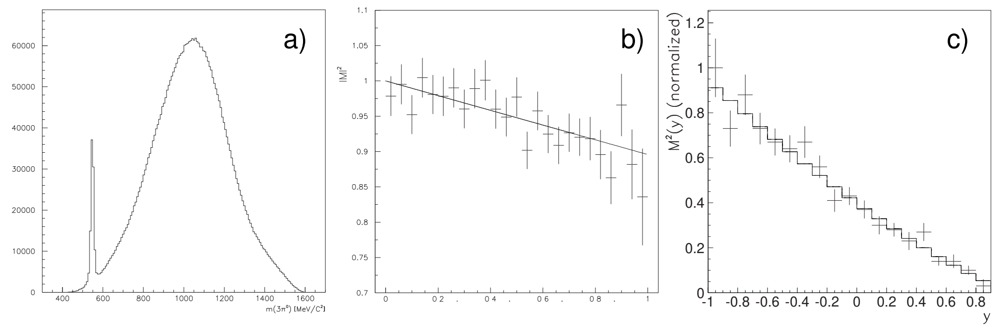

FIGURE 8. a) The invariant $3\pi^0$ mass in the process $\bar{p}p \to 5\pi^0$ b) The z-distribution from $\eta \to 3\pi^0$ after subtraction of the background and acceptance correction. c) Phase space normalized projection of the $\eta \to \pi^+\pi^-\pi^0$ Dalitz plot ($y = 3T_0/Q - 1$, where T_0 is the kinetic energy of the π^0 and $Q = m_\eta - 2m_{\pi^+} - m_{\pi^0}$).

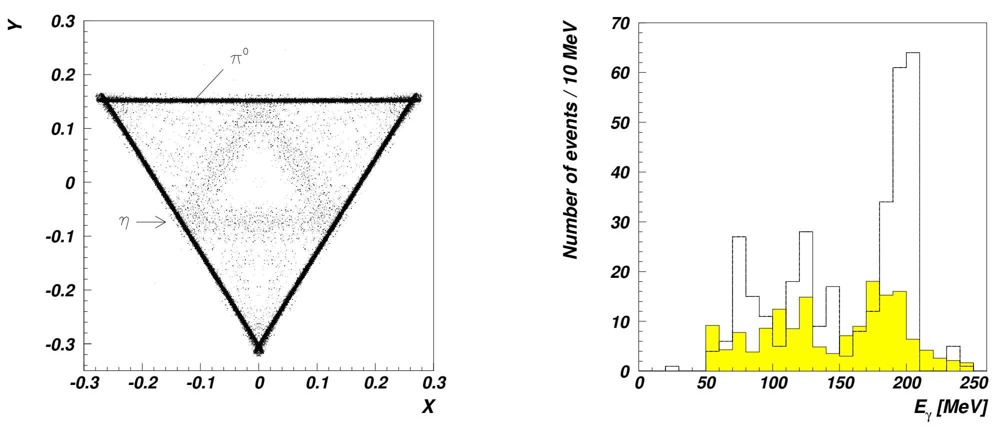

FIGURE 9. a) $\omega \to 3-\gamma$ Dalitz plot for the reaction $\bar{p}p \to \pi^0\omega$ (6 entries/event). b) γ energy distribution in the ω rest frame for $\eta\omega(\omega \to 3\gamma)$ events outside the π^0 band. Ploted is the γ with the lowest energy. The shaded histogram shows the background from $2\eta\pi^0$ (where one γ escaped detection).

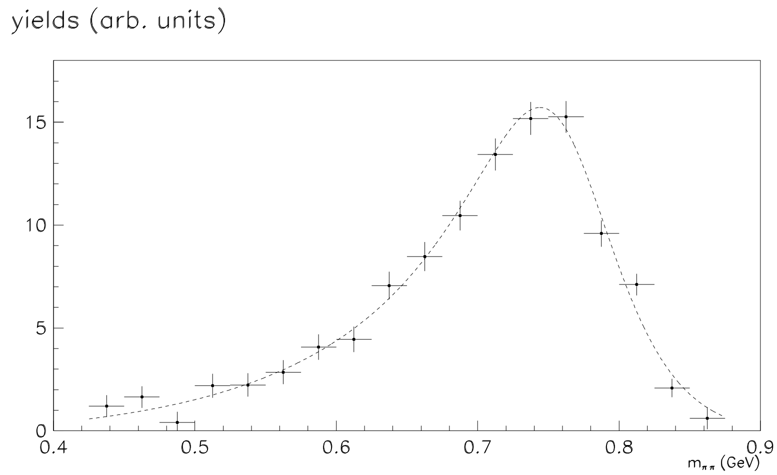

FIGURE 10. $m(\pi^+\pi^-)$ distribution in the decay $\eta' \to \pi^+\pi^-\gamma$. Crystal Barrel data are shown as crosses together with the result of the fit with model M_2 (dashed line); the fit quality using M_1 is identical.

(62,853 events) shows clear signals for the $\pi^0\gamma$ and $\eta\gamma$ decay modes of the ω. Using the known branching ratio $B(\omega \to \pi^0\gamma) = (8.5 \pm 0.5)$ % [16], a value for $B(\omega \to \eta\gamma)$ of $(6.5 \pm 1.1) \times 10^{-4}$ is obtained for the production channel $\bar{p}p \to \eta\omega$, while a value of $(13.1 \pm 2.4) \times 10^{-4}$ is obtained in the production channel $\bar{p}p \to \pi^0\omega$. The discrepancy is explained by the effect of $\rho - \omega$ interference, which mainly affects the second channel. If this effect is taken into account, a value of $(6.6 \pm 1.7) \times 10^{-4}$ for both production channels is obtained [17], consistent with constructive interference. This value is in good agreement with that of [18], which was obtained in the reaction $\pi^- p \to \omega n$ at large momentum transfers, thus suppressing ρ production.

Based on 7392 η' decays in several different reactions ($\bar{p}p \to \omega\eta'$, $\bar{p}p \to \pi^0\pi^0\eta'$ and $\bar{p}p \to \pi^+\pi^-\eta'$), the $\pi^+\pi^-$ invariant mass distribution from η' decays into $\pi^+\pi^-\gamma$ has been studied [19]. This dipion mass spectrum is dominated by the ρ^0, but an additional non-resonant contribution – which might be identified with the box anomaly expected from current algebra and chiral theories [20] – has been identified in a combined study of 9 existing data sets (with a total of about 8000 events). In addition to systematic effects coming from combining a number of different experiments, any measurement of box anomalies relies on the model used to describe the ρ meson. Two models of the ρ meson (both giving a good description of the $e^+e^- \to \pi^+\pi^-$ data) are used to fit the dipion mass distribution of Fig. 10. This spectrum is obtained by determining the number of η' events for each 25 MeV/c^2 $m(\pi^+\pi^-)$ mass window for each of the reactions in which Crystal Barrel observes the η'. One then corrects for the dipion mass-dependent and reaction-dependent detection efficiency, and obtains the total number of η' for that dipion mass window. For both parametrizations of the ρ, the fit to the data confirms the presence of a box-anomaly term in η' decay to $\pi^+\pi^-\gamma$ at a level consistent with predictions from [21], and with a statistical significance (dependent on the ρ parametrization used) of at least 4 σ. The presence of systematic differences between the different reactions was also investigated; all differences between the fit results of the different subsamples are consistent with statistics only.

REFERENCES

1. C. Amsler et al. (Crystal Barrel Collab.), Phys. Lett. B 355 (1995) 425 and references therin.
2. M. Doser et al., submitted to Nucl. Inst. Meth.
3. A. Abele et al.(Crystal Barrel Collab.), Phys. Lett. B 385 (1996) 425.
4. L. Gray et al., Phys. Rev. D 27 (1983) 307.
5. J. Gasser and H. Leutwyler, Nucl. Phys. B 250 (1985) 539.
6. J. Kambor, C. Wiesendanger and D. Wyler, Nucl. Phys. B 465 (1996) 215.
7. M. Gormley et al., Phys. Rev. D 2 (1970) 501.
8. J.G. Layter et al., Phys. Rev. D 7 (1973) 2565.
9. A. Abele et al. (Crystal Barrel Collab.), submitted to Phys. Lett. B
10. A. Abele et al. (Crystal Barrel Collab.), submitted to Phys. Lett. B
11. H.B. O'Connell et al., Rev. Mod. Phys. 53 (1981) 673,
    R. Sekhar Chivukula and J.M. Flynn, Phys. Lett. B 168 (1986) 127.
12. H.B. O'Connell et al., Phys. Lett. B354 (1995) 14.
13. D. Alde et al., Z. Phys. C25 (1984) 225.
14. C. Baglin et al., Nucl. Phys. B22 (1970) 66.
15. C. Amsler et al.(Crystal Barrel Collab.), Z. f. Physik C58 (1993) 175.
16. Particle Data Group: Review of Particle Physics, Phys. Rev. D54 I (1996) 1.
17. A. Abele et al. (Crystal Barrel Collab.), Phys. Lett. B411 (1997) 361.
18. D. Alde et al., Z. Phys. C61 (194) 35.
19. A. Abele et al. (Crystal Barrel Collab.), Phys. Lett. B402 (1997) 195.
20. M. Benayoun et al., Z. f. Phys. C58 (1993) 31.
21. M.S. Chanowitz, Phys. Rev. Lett. 35 (1975) 977, Phys. Rev. Lett 44 (1980) 59.
    R. Akhoury and J.M. Frère, Phys. Lett. B220 (1989) 258.